

Error Analysis of Spectral Reflectance Derived from Imaging Spectrometer Data¹

John P. Kerekes

Lincoln Laboratory, Massachusetts Institute of Technology
244 Wood St., Lexington, Massachusetts 02173
kerekes@ll.mit.edu

ABSTRACT

As the field of remote imaging spectrometry grows, interest increases in applications that require the data be "corrected" to surface reflectance. However, the utility of the data for these applications will be limited by the accuracy to which the correction can be performed. Two approaches to atmospheric compensation are reviewed and applied to airborne spectrometer data to study their error characteristics. An end-to-end analysis model is used to extend the study to examine the effects of individual sources of error. Results indicate that random errors of 1 to 2% reflectance units and bias errors of 1 to 4% are achievable in atmospheric window regions, with considerably higher errors in atmospheric absorption bands.

INTRODUCTION

A number of applications of remote imaging spectrometry require the data be "corrected" (compensated) for illumination and atmospheric effects. The retrieved surface reflectance is used to identify materials either by individual spectral absorption features, or by matching the overall spectral shape to samples from libraries. However, the utility of the data for these applications is limited by the accuracy to which the atmospheric compensation can be performed. Understanding the sources and magnitudes of corrupting influences on this process is important in assessing the robustness of various compensation algorithms.

This paper addresses system effects on the error by studying the error characteristics of two atmospheric compensation approaches: a linear correction technique based on knowledge of reflectances in the scene, and a radiative transfer approach which uses a physical model to compensate for the solar illumination and the atmosphere.

The context considered is one of high spatial resolution airborne or spaceborne imaging spectrometers (hyperspectral sensors) sensing surface reflected sunlight in the visible through shortwave infrared spectrum. The objects of interest on the surface will be assumed to be in the open, not occluded by trees or other objects, and to occupy at least one whole pixel in the image. Complications resulting from multiple scattering, as in a forest, are not considered.

ILLUMINATION AND ATMOSPHERIC EFFECTS

Before addressing surface reflectance retrieval, it is relevant to discuss the illumination and atmospheric effects that are present in the remotely sensed measurement. Figure 1 shows the various significant paths for the radiance measured by an airborne or spaceborne imaging spectrometer for a flat, nearly homogeneous background scene with an isolated, extended object, but without effects due to foliage obscuration, vertical relief, or manmade objects.

Four significant terms are seen to form the total radiance incident at a sensor aperture: L_{Dir} , the directly reflected radiance for a single path from the Sun to the object of interest and into the sensor; L_{Diff} , the sky or diffuse radiance reflected by the object; L_{Back} , the radiance reflected by the nearby background and scattered into the sensor field-of-view (sometimes referred to as the *adjacency effect*, although that term is also used to describe the reflected flux onto an object by adjacent structures - a term not considered here); and L_{Path} , the atmospheric scattered path radiance. All terms are functions of wavelength, as well as geometry and spatial coordinates.

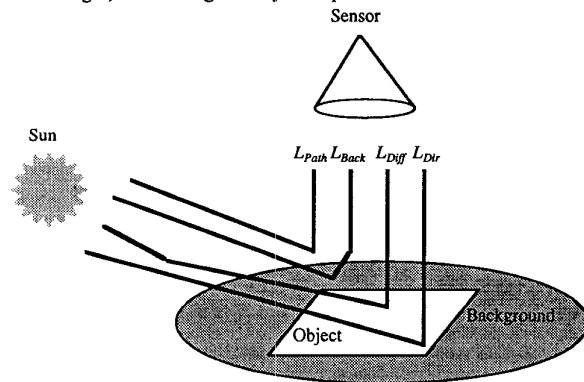


Figure 1. Significant paths of reflected sunlight incident at sensor.

Analytical equations governing these components can be found in [1] with the exception of the L_{Back} term. This term is sometimes included in the L_{Path} term through multiple scattering effects and the interactions between the atmosphere and the surface boundary. The L_{Back} term is differentiated here to emphasize it as a potential source of error if not properly accounted for in the retrieval.

Discrete approximations to the analytical equations have been made in several computer programs including Modtran [2]. A good approximation to the total at-sensor radiance can be made by adding the results from two Modtran runs. One, using the reflectance spectrum of the object as the surface albedo, will produce the sum $L_{Dir}+L_{Diff}$ labeled as "total ground reflected radiance". A second run, using the background reflectance spectrum as the surface albedo, will produce the sum $L_{Path}+L_{Back}$ labeled as "path scattered radiance".

It has been found that the accurate calculation of the sky or diffuse contribution to the surface illumination when using Modtran requires a number of runs and a numerical integration [3]. However, the error introduced by the simplified two-run procedure above is small and limited to the extreme short wavelength end of the spectrum where atmospheric scattering is most significant.

¹ This work was sponsored by the Department of Defense under Air Force contract F19628-95-C-0002. Opinions, interpretations, conclusions, and recommendations are those of the author and not necessarily endorsed by the United States Air Force.

Regarding the use of the term “reflectance”, while the Bidirectional Reflectance Distribution Function (BRDF) is the most general way of describing reflectance, it is common to use a unitless reflectance factor, r , which is π times the BRDF and to make the assumption that the surface is Lambertian. While errors do arise from this assumption [4], they will not be considered further here, and throughout this paper we will use the term reflectance to mean the reflectance factor for a perfectly diffuse surface.

RETRIEVAL OF SURFACE REFLECTANCE

Algorithms for the retrieval of the surface reflectance can be grouped into three types: in-scene, ground-truth, and radiative transfer models.

In-scene approaches do not rely on any ancillary information and can even be applied to uncalibrated data. They usually produce a relative reflectance which can be useful for distinguishing materials of different types, or possibly even identifying materials that have unique spectral features very distinct from atmospheric absorption bands or spectra of other materials in the scene. While these approaches have many applications, they do not produce an absolute reflectance spectra which could be compared to laboratory or previous measurements and are not considered in this study.

Ground truth methods rely on having objects in the remotely sensed image for which the spectral reflectance is known, either through laboratory measurements, or measured on the ground at the same time as the remotely sensed image. The model assumed is

$$L_{sensor} = \frac{1}{\pi} [E_S + E_D] \tau r + L_{path} \quad (1)$$

where E_S and E_D are the irradiance incident on the surface due to the direct solar and diffuse sky sources, τ is the transmittance of the atmosphere from the surface to the sensor, r is the surface reflectance factor, and L_{path} is the scattered solar radiance from the atmosphere, as well as from the nearby background. The estimate of the surface reflectance is then usually obtained by linear regression for several known reflectance values (as a function of wavelength) yielding the following equation where G and O are often referred to as the *gain* and *offset* for the retrieval.

$$\hat{r} = G L_{sensor} + O. \quad (2)$$

This approach has several limiting assumptions including a constant atmosphere over the image, and that the reference objects and the targets of interest have the same reflectance characteristics (e.g., both Lambertian). While this technique does not require an accurate absolute sensor radiance calibration, it is sensitive to any nonuniformity across the sensor array, or errors in the relative calibration. Also, the accuracy of this approach will be limited by the accuracy of the field measurements for the reference objects as well as their uniformity over the range of spatial scale from the ground measurement to the remotely sensed measurement.

Radiative transfer models retrieve reflectance by accounting for all physical effects that contribute to the at-sensor radiance measurement. Ideally, one would like to know the precise illumination and observation geometry, the solar illumination level,

the exact concentrations of atmospheric gases (including water vapor, the most variable and dominant in this spectral region), the concentrations and scattering phase functions of aerosols and molecules, and the reflectance of the nearby backgrounds. Practically, one usually has some information about these details and the rest are derived from the remotely sensed image. This is one application where imaging spectrometers with their hundreds of contiguous spectral bands (including atmospheric absorption bands) have an advantage over traditional multispectral sensors which do not collect data in the absorption bands.

It is important to note, however, that techniques based on radiative transfer modeling require accurately calibrated sensor radiance, and any errors in the absolute calibration will directly affect the retrieved reflectance.

One example of a radiative transfer code is ATREM [5]. Originally designed for application to data collected by NASA’s AVIRIS sensor, it uses measurements around weak water vapor absorption bands to derive estimates of the column water vapor on a pixel-by-pixel basis. The effects due to the solar illumination geometry, fixed atmospheric gases, aerosols and molecular scattering, are determined through a combination of input parameters and use of the 6S atmospheric code [6]. These components, along with the derived water vapor, are then used to retrieve the surface reflectance. Radiative transfer algorithms have also been built around Modtran including those at JPL [7], and Spectral Sciences [8].

ANALYSIS OF HYDICE DATA

To assess the surface reflectance retrieval accuracy achievable with the airborne HYDICE [9] imaging spectrometer, two scenes were analyzed. Table 1 gives details of the selected scenes. Both scenes contained large (9 m x 9 m) radiometric calibration panels of varying reflectance used for the ground truth method. Also common in both scenes were several uniform reflectance panels (3 m x 3 m) that were deployed at each site; four of which are used in this study as test objects. Figure 2 shows an image of the Aberdeen site. The radiometric calibration panels are the stepwise-varying (2%, 4%, 8%, 16%, 32%, and 64% reflectance) gray-level objects. The smaller test panels are arranged in a regular pattern above the calibration panels in the image.

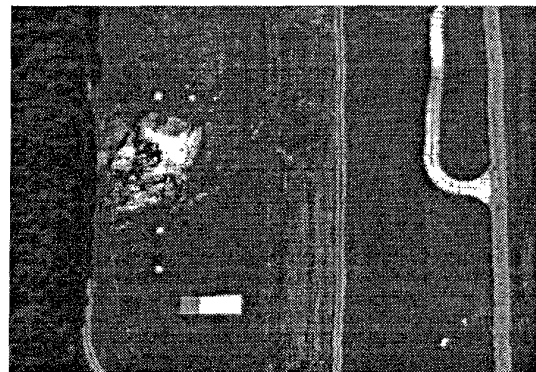


Figure 2. Aberdeen HYDICE scene used in analysis.

Table 1. HYDICE scenes used in analysis.

Location	Date	Local Time	Sensor Altitude	Ground Resolution
Yuma, AZ	26 June 1995	8:51 AM	1500 m	~0.75 m
Aberdeen, MD	24 August 1995	9:10 AM	1500 m	~0.75 m

Both ground truth (Empirical Line Method or ELM) and radiative transfer (HYDICE version of ATREM) algorithms were applied to the scenes. Figures 3 and 4 show example results comparing the field spectrometer ground measurement (convolved with the HYDICE spectral response) to the retrieved reflectance for a single pixel of two of the smaller panels in the Aberdeen scene. The major spectral features are clearly retrieved with either technique.

To statistically assess the error in the retrieved reflectances, pixels from four of the calibration panels and the four test panels from each scene were compared against the ground truth. Figures 5 and 6 show the systematic bias and standard deviation of the random error using a total of 80 pixels. Both techniques show an error standard deviation of 1 to 2% reflectance units, except for the water vapor absorption bands at 0.94, 1.13, 1.4, and 1.9 μm , and where the sensor signal-to-noise ratio (SNR) is low. However, the radiative transfer method error is generally higher throughout the spectrum. The radiative transfer algorithm also has several regions of increased bias error, including: the short wavelength portion where scattering dominates, the weak water vapor bands at 0.94 and 1.13 μm , and the region above 2.0 μm . These bias errors are most likely due to incorrect assumptions of the atmospheric haze and errors in determining the water vapor content, as well as residual absolute calibration error in the HYDICE data. The ELM method doesn't require knowledge of those parameters; the method just compensates for those effects, and as a result its bias is fairly flat.

Figures 7 and 8 present two different error correlation coefficients for the two techniques. The *spectral* error correlation is the correlation between the error in retrieved reflectance of each spectral channel and its adjacent channel. This represents a measure of how well the algorithm maintains the integrity of the shape of the surface spectral reflectance. The *spatial* error correlation is a measure of the consistency of the error from pixel-to-pixel. The radiative transfer algorithm ATREM shows a higher error correlation of both types. In all cases, the correlation decreases at the edge of water vapor absorption bands as well as in regions of low SNR.

The next two figures address sources of error in the retrieval process. Figure 9 plots for three example wavelengths the ground measurements of the calibration panel reflectance against the HYDICE radiance averaged over the panels, along with best fit lines. For this example, the fit looks very good and any error due to non-linearity is less 1% in reflectance units.

Figure 10 shows the ground measurements and the ATREM retrieved reflectance for three of the spectrally flat calibration panels in the Aberdeen scene. Careful examination shows a residual vegetation spectrum consistent among the different panel curves. This spectral component (green peak, red absorption, high near-infrared) originates from radiance scattered by the atmosphere from the nearby grass and forested areas (L_{Back}) into pixels that are assumed to contain only the calibration panels. (A non-ideal sensor

spatial response may also contribute to this effect.) Since this retrieval algorithm does not consider the scattering from the background, the algorithm returns a reflectance contaminated by the background. The magnitude of this type of error will depend on the relative contrast between the object of interest and the background, the scattering phase functions, and amounts of aerosols in the atmosphere. As evident in Fig. 10, the error can be significant and could prevent the proper identification of small objects.

ERROR SOURCES AND MODEL ANALYSES

The above examples illustrate some of the effects that lead to errors in retrieved spectral reflectance; however, there are many more such sources. Building on earlier work [10], Table 2 lists a number of sources of error in the surface reflectance retrieval problem. The sources listed in italics will be discussed further.

Table 2. Error sources and their impact on the two methods studied.

Error Source Impact on error statistics in \Rightarrow	Grnd. Truth			Rad. Trans.		
	Bias	SD	Corr.	Bias	SD	Corr.
Scene						
<i>Water vapor variation</i>	✓	✓	✓			
Local aspect and slope	✓			✓		
BRDF effects	✓			✓		
Sensor						
<i>Spectral calibration</i>				✓	✓	✓
<i>Abs. radiometric calibration</i>				✓		✓
<i>Radiometric random noise</i>		✓			✓	
<i>Radiometric nonuniformity</i>		✓	✓		✓	✓
Modulation transfer function	✓		✓	✓		✓
Linearity of sensor response	✓		✓	✓		✓
Sensor instability		✓			✓	
Processing						
Reference spectra errors	✓					
Reference variability	✓					
Reference nondiffuseness	✓					
Linearity of radiative transfer	✓		✓			
Inaccurate solar irradiance				✓		✓
Fixed gas concentration error				✓		✓
Incorrect water vapor retrieved				✓		✓
Incorrect scattering model				✓		✓
Neglecting of background term				✓		✓

The impact on error statistics of each of the various error sources is noted in Table 2 to give an idea of how they can affect the utility of the retrieved reflectances. Bias errors will affect all pixels in a scene equally and will potentially mask spectral features useful in identifying surface materials. Random errors will affect the error standard deviation which also may mask spectral features, but more significantly may reduce the separability between different ground object classes. Correlations in the error statistics will also affect separability by introducing false relationships between the spectral channels that may mislead some identification algorithms. The ultimate impact on utility of these errors can only be considered in the context of particular applications and algorithms.

It is also important to note that these error sources are not all necessarily statistically independent. Bias errors could be of either sign and could conceivably cancel one another out. Random errors of one type could exacerbate errors of another. Thus, the usual root-mean-square rule for combining errors will not generally hold and each situation must be considered individually.

However, to assess the typical sensitivity of retrieved reflectance accuracy to individual error sources, a model using Modtran as described earlier, together with additional models for sensor effects, was used to study the parameters listed in italics in Table 2. The model was configured to duplicate conditions for the Aberdeen run described above with a 16% calibration panel as the ground object.

Water vapor variation. In using the ground truth method (ELM), a difference in the amount of atmospheric water vapor in the part of the scene where the calibration panels are located as compared to where the objects of interest are located, will lead to errors in the retrieved reflectance. Figure 11 shows the impact on retrieved reflectance due to 54% more (dotted) or 44% less (solid) water vapor at the objects of interest. The effect is most significant in the regions of water vapor absorption, but those regions are fairly broad.

Spectral calibration. A characteristic of the HYDICE sensor is that the central wavelength of each channel can vary from line-to-line in the image due to mechanical vibrations. This effect, known as spectral jitter, affects the utility of the data when applying radiative transfer algorithms such as ATREM. Figure 12 shows the effect on ATREM retrieved reflectance of a misalignment between the actual and the assumed central wavelengths by ± 1 and ± 2 nm, a typical amount seen in the sensor. These results show the retrieved reflectance can be significantly affected in regions around atmospheric absorption lines where much spectral structure exists. Atmospheric window regions of high transmittance are less affected.

Absolute calibration error. As mentioned earlier, radiative transfer codes, such as ATREM, are also subject to errors from inaccurate absolute calibration. Figure 13 shows the fractional change in retrieved reflectance as a function of a fractional error in the absolute calibration for three example wavelengths. The sensitivity is linear and nearly exactly proportional, but with a slightly different slope for each wavelength. In the blue region ($0.428 \mu\text{m}$), dominated by atmospheric scattering, the slope is the greatest indicating the most sensitivity to absolute calibration.

Random noise or nonuniformity. All retrieval methods will be affected by random errors in the measurement which include sensor radiometric noise as well as residual focal plane nonuniformity correction (NUC) errors. Figure 14 shows for three example wavelengths (chosen to span the range of sensitivity), the sensitivity of errors in the retrieved reflectance to random radiometric errors (added at all wavelengths) with a standard deviation expressed as a percentage of the signal. (A 2% random noise standard deviation is equivalent to a SNR of 50). The sensitivity varies for the different wavelengths and the two methods with the biggest difference occurring for the weak water vapor absorption line at $1.128 \mu\text{m}$. Here, the ATREM results are more than twice as sensitive as ELM to random errors. This is not unexpected since the correction at this wavelength is dependent upon the retrieved water vapor which will be very sensitive to noise in the measurements.

SUMMARY AND CONCLUSIONS

Issues associated with the retrieval of surface reflectance from imaging spectrometer data have been discussed along with a brief description of common retrieval algorithms. Examples of the typical accuracy and types of error sources have been given. Observations on real data were extended by applying model simulations to study the sensitivity of several system parameters.

Outside of the water vapor absorption bands, random errors of 1% to 2% reflectance factor units and systematic bias errors of 1% to 4% were observed. The ground truth method ELM achieved smaller errors than the radiative transfer model ATREM, although the performance of ATREM was limited in part by spectral and radiometric calibration errors in the HYDICE data. The impact on retrieval accuracy of these and other error sources was studied parametrically through a model with results consistent with the HYDICE data analyses.

Ultimately, the impact of reflectance retrieval errors on the utility of imaging spectrometer data will depend upon the application and the algorithm used to extract the desired information from the data.

REFERENCES

- [1] J.R. Schott, **Remote Sensing: The Image Chain Approach**, Oxford University Press, New York, NY, 1997.
- [2] A. Berk, L.S. Bernstein, D.C. Robertson, "MODTRAN: a moderate resolution model for LOWTRAN 7," GL-TR-89-0122, Spectral Sciences, Burlington, MA, 1989.
- [3] W. Stoner, SAIC, Burlington, MA, personal communication.
- [4] T.Y. Lee and Y.J. Kaufman, "Non-Lambertian Effects on Remote Sensing of Surface Reflectance and Vegetation Index," *IEEE Trans. on Geo. Rem. Sens.*, Vol. 24, No. 5, pp. 699-708, Sept. 1986.
- [5] B.-C. Gao, K.B. Heidebrecht, A.F.H. Goetz, "Derivation of Scaled Surface Reflectances from AVIRIS Data," *Rem. Sens. Env.*, Vol. 44, pp. 165-178, 1993.
- [6] E.F. Vermote, D. Tanre, J.L. Deuze, M. Herman, J.J. Morcrett, "Second Simulation of the Satellite Signal in the Solar Spectrum: An Overview," *IEEE Trans. on Geo. Rem. Sens.*, Vol. 35, No. 3, pp. 675-686, May 1997.
- [7] R.O. Green, D.A. Roberts, J.E. Conel, "Characterization and Compensation of the Atmosphere for the Inversion of AVIRIS Calibrated Radiance to Apparent Surface Reflectance," *Proceedings of the Sixth Annual JPL Airborne Earth Science Workshop*, NASA/JPL, 4 March, 1996.
- [8] S. Adler-Golden, A. Berk, L.S. Bernstein, S. Richtsmeier, "Flaash: A Modtran4 Atmospheric Correction Package for Hyperspectral Data Retrievals and Simulations," *Proc. of the 7th Annual JPL Airborne Earth Science Workshop*, 12 January 1998.
- [9] L.J. Rickard, et al, "HYDICE: An Airborne System for Hyperspectral Imaging," *SPIE Proc. Imaging Spectrometry of the Terrestrial Environment*, v. 1937, p. 173, 1993.
- [10] J.P. Kerekes, and D.A. Landgrebe, "A Noise Taxonomy for Remote Sensing Systems," *Proc. IGARSS '87*, pp. 903-908, Ann Arbor, Michigan, 18-21 May, 1987.

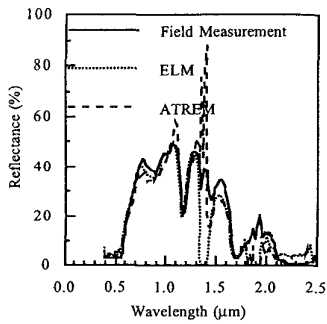


Fig. 3. Reflectance of rust-colored plastic.

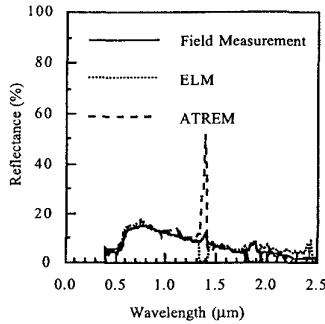


Fig. 4. Reflectance of brown fibreglass.

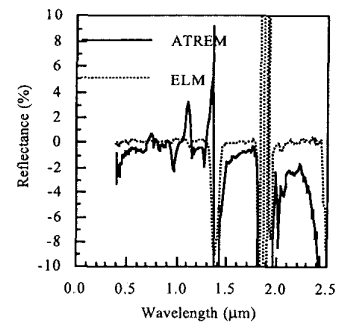


Fig. 5. Bias error for all test pixels.

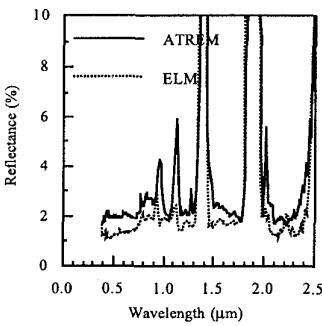


Fig. 6. Std. dev. of error for all test pixels.

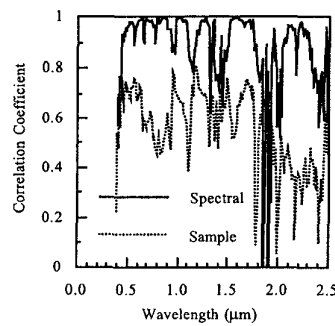


Fig. 7. Error correlation for ELM. See text.

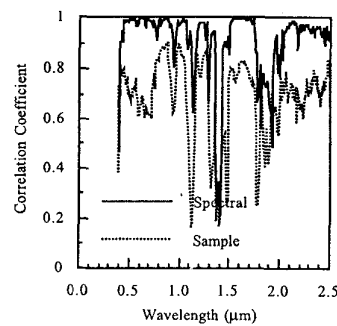


Fig. 8. Error correlation for ATREM. See text.

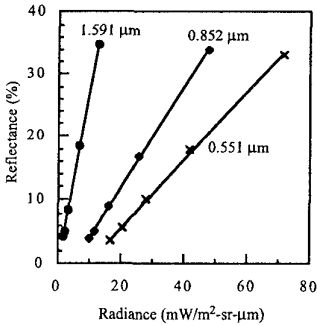


Fig. 9. Linearity of radiance to reflectance.

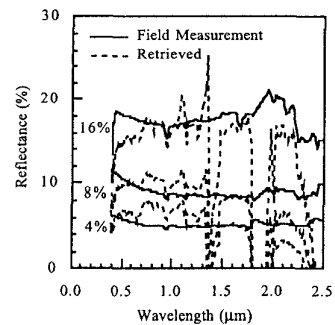


Fig. 10. Residual grass spectra seen in ATREM retrieved cal. panel reflectance.

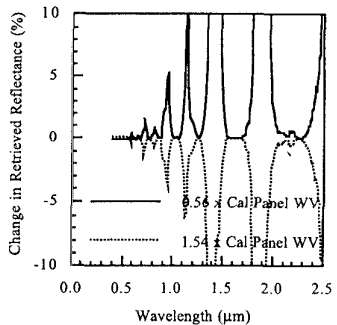


Fig. 11. Effect of varying water vapor in area away from ground truth panels.

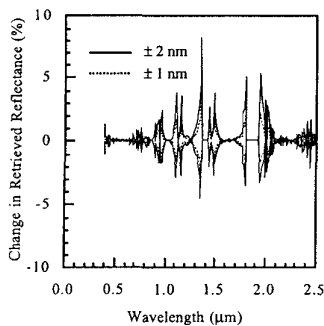


Fig. 12. Effect of channel spectral shift on ATREM retrieved reflectance.

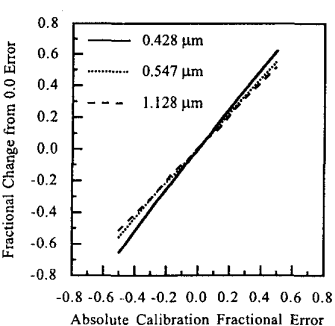


Fig. 13. Relationship of absolute radiance error to error in ATREM retrieved reflectance.

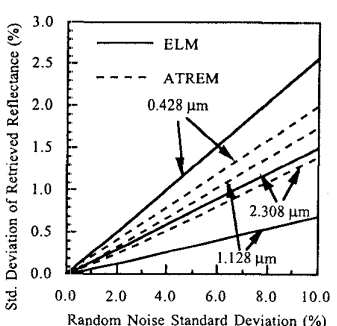


Fig. 14. Relationship of random error in radiance to error in retrieved reflectance.